Supporting information

Three-dimensional porous Gd-POMs/RGO composites for high-performance supercapacitor electrodes

Fei Fei[a], Shuai Wang[a], Lanqin He[a], Pushan Wen[b,*]

[a]*Department of Chemistry and Chemical Engineering, Zunyi Normal College, Zunyi 563006, Guizhou, China*

[b]*Department of Chemistry and Environmental Engineering, Guizhou Industry Polytechnic College, Guiyang, 550008, Guizhou, China*

*Corresponding author. E-mail address: wenpushan@126.com (P. Wen).

Characterization

The morphologies and elemental analyses were conducted using Field Emission Scanning Electron Microscopy (FESEM, JEOL-7610F Plus) equipped with Energy Dispersive Spectroscopy (EDS), and Transmission Electron Microscope (TEM, FEI Titan G2 60-300). The crystalline phases of the products were analyzed via X-ray diffraction (XRD, Philips X'pert diffractometer). Fourier Transform Infrared (FTIR-7600 lambda) spectroscopic analysis were used to examine the chemical bonds. The Raman analysis was conducted using Bruker Multi RAM equipment. The chemical structure and elemental information were detected via X-ray photoelectron spectroscopy (XPS, VG Scientific Ltd ESCALAB MK II). The Brunauer–Emmett–Teller (BET) surface area was measured using a Micromeritics instrument (ASAP 2020) in a liquid nitrogen atmosphere. The contact angle of the sample was measured using a contact angle measuring instrument (Theta Flex, sessile drop). The surface electrical properties of the materials were measured using a zeta potential analyzer (ZEECOM ZC2000, Microtec, Chiba, Japan).

Electrochemical measurements

The Bio-Logic SP-300 electrochemical workstation was used for the electrochemical evaluations, including cyclic voltammetry (CV), galvanostatic charge-discharge (GCD), and electrochemical impedance spectroscopy (EIS) in 2 M KOH electrolyte. Ag/AgCl and platinum plate were used as reference and counter electrodes, respectively. The working electrodes were prepared as follows: the as-synthesized samples, carbon black, and polyvinylidene fluoride (PVDF) were dispersed in N-

methyl-2-pyrrolidinone with a mass ratio of 8:1:1, and the resulting slurry was cautiously coated on the nickel foam substrates (1 cm×1 cm). After that, the nickel foams were dried at 70 °C for 12 h under vacuum. The mass loading of active materials was ~3 mg cm^{-2}. Besides, an asymmetric supercapacitor (ASC) cell was manufactured using Gd-POMs/RGO (cathode) and activated carbon (anode) with 2 M KOH as the electrolyte. The mass ratio between the two electrodes (m_+/m_-) can be optimized according to the following equation:

$$\frac{m_+}{m_-} = \frac{C_- \times \Delta V_-}{C_+ \times \Delta V_+} \quad \text{(S1)}$$

where C_s (F g^{-1}), ΔV (V) and m (g) are the specific capacitance, voltage window and mass of active materials, respectively.

The specific capacitance (C_s, F g^{-1}), energy density (E, W h kg^{-1}), and power density (P, W kg^{-1}) can be calculated according to the following equations:

$$C_s = \frac{I \times \Delta t}{m \times \Delta V} \quad \text{(S2)}$$

$$E_s = \frac{C_s \times \Delta V^2}{2 \times 3.6} \quad \text{(S3)}$$

$$P_s = \frac{3600 \times E}{\Delta t} \quad \text{(S4)}$$

where I (A), ΔV (V), Δt (s) and m (g) represent the current, voltage window, discharge time and mass of active materials, respectively.

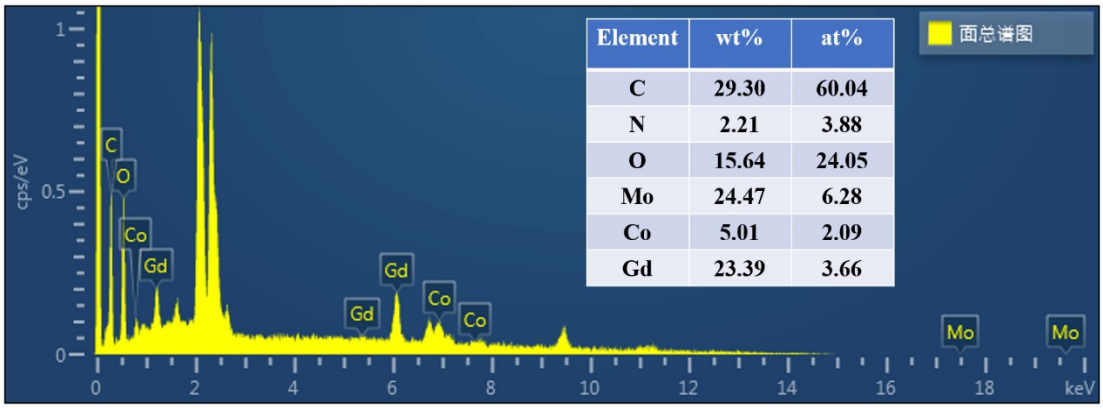

Fig. S1 EDX spectrum of Gd-POMs/RGO.

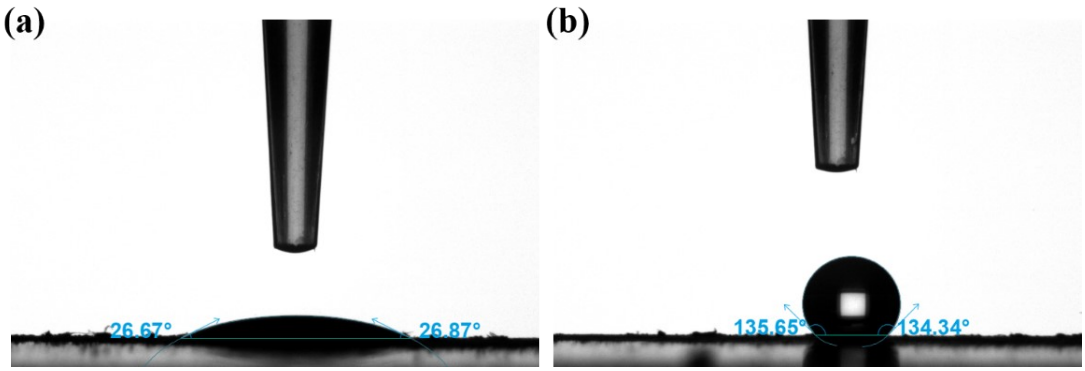

Fig. S2 Water contact angle of a) POMs, b) Gd-POMs/RGO.

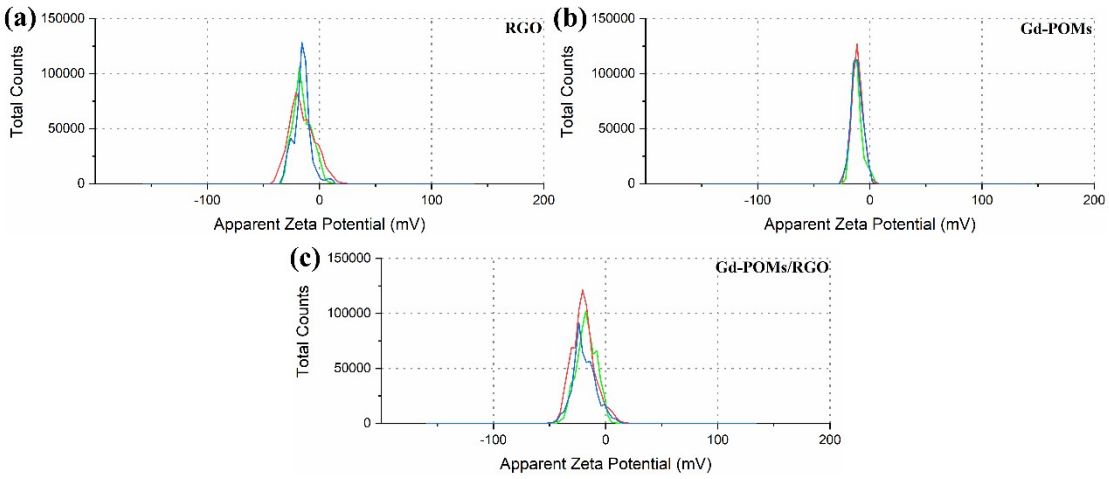

Fig.S3 Zeta potential analysis of (a) RGO, (b) Gd-POMs, and (c) Gd-POMs/RGO.

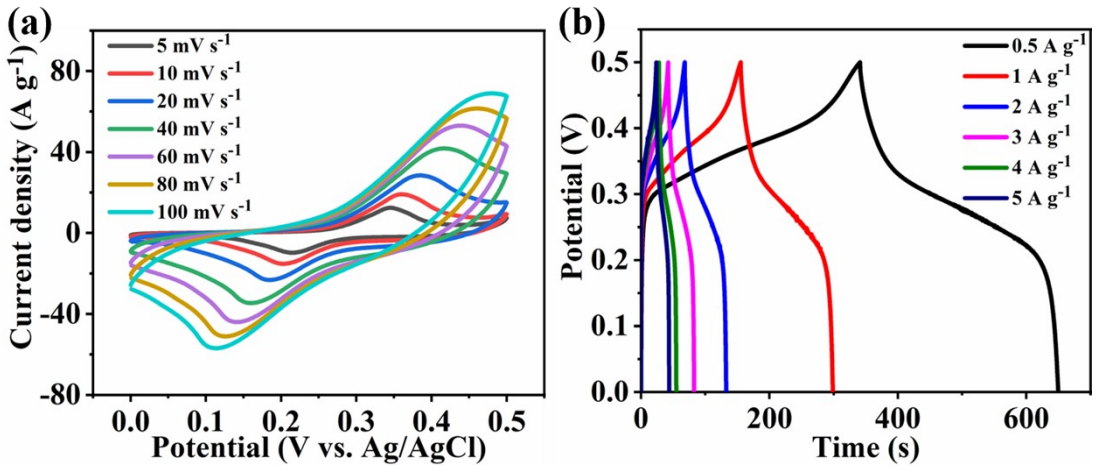

Fig. S4 (a) CV curves and (b) GCD curves of Gd-POMs.

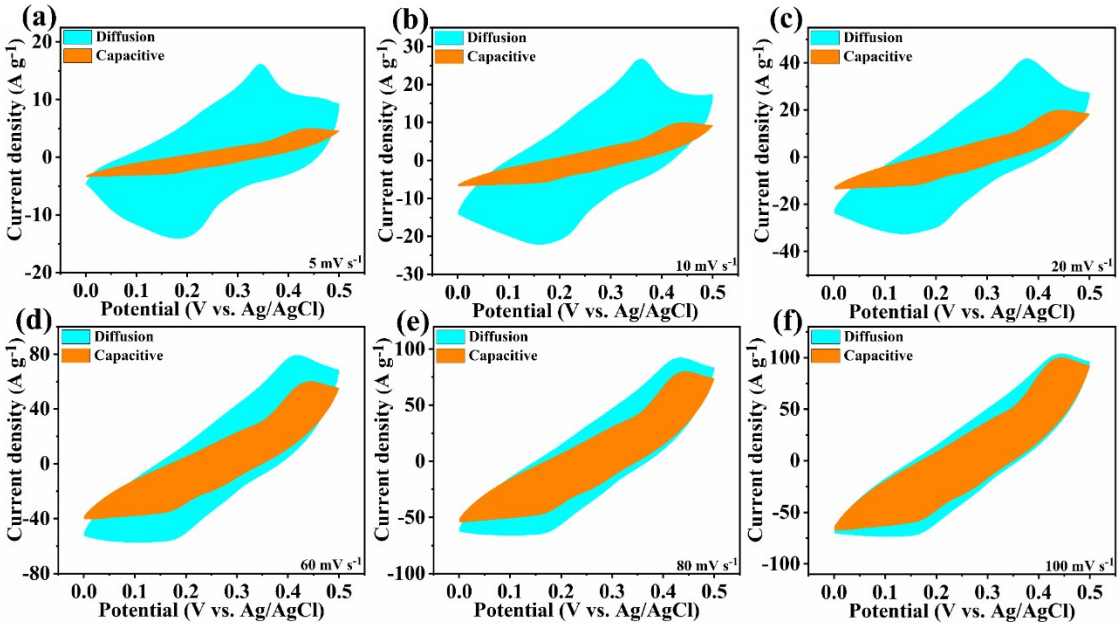

Fig. S5 The analysis of capacitive- and diffusion-controlled contribution of Gd-POMs/RGO at various scan rates of 5–100 mV s^{-1}.

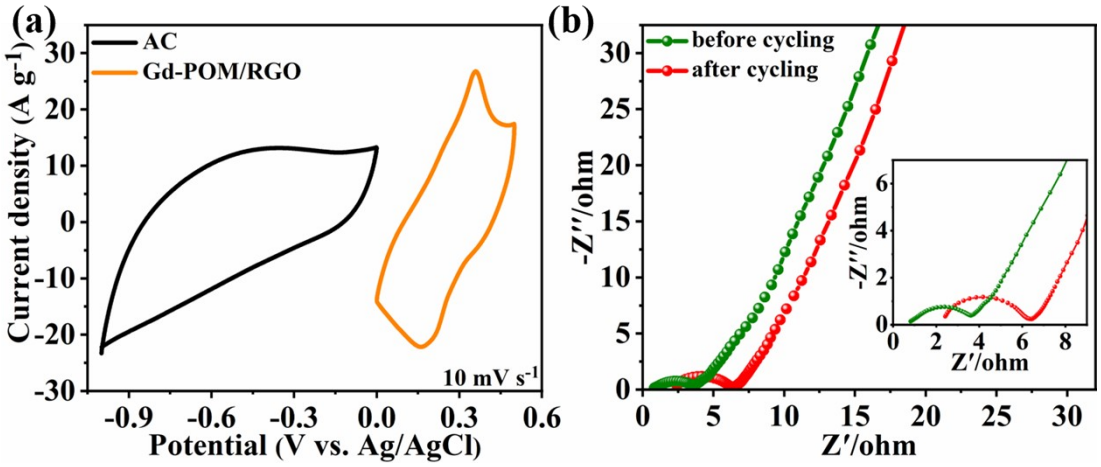

Fig. S6 (a) CV curves of Gd-POMs/RGO and AC at 10 mV s^{-1}. (b) EIS curve recorded before and after cycling test of the assembled Gd-POMs/RGO//AC cell.

Table S1. Comparison of the electrochemical performance with some previously reported SC cells based on POMs.

SC cells	E (W h kg^{-1})	P (W kg^{-1})	Ref.
Gd-POMs/RGO//AC	53.06	749.73	This work
PAHB-9/RGO//PAHB-9/RGO	26.2	600	[1]
rGO-PMo_{12}//rGO-PW_{12}	39	658	[2]
Ni/Mn-PMo_{12}//AC	28.3	375	[3]
PW_{12}@MIL-101/PPy//PW_{12}@MIL-101/PPy	20.7	277.6	[4]
PMo_{12}@PPy//PMo_{12}@PPy	22.9	706	[5]
SWCNT-TBA-PV_2Mo_{10}//SWCNT-TBA-PV_2Mo_{10}	15.4	15700	[6]
PPy/PMo_{12}//PEDOT/PW_{12}	4	103	[7]
10-PMo_{12}/SSAC-OP//10-PMo_{12}/SSAC-OP	23.91	1016.05	[8]
CNT/PMo/PANI//CNT/PMo/PANI	18.7	2000	[9]
mAC//Mo_{132}-rGO	31.6	207.7	[10]

References

1 G. Fan, L. J. Deng and Y. Z. Gu, *Sustainable Energy Fuels*, 2021, **5**, 1892-1903.

2 D. P. Dubal, N. R. Chodankar, A. Vinu, D.-H. Kim and P. Gomez-Romero, *Chemsuschem*, 2017, **10**, 2742-2750.

3 M. J. Huang, P. C. Wang, Y. Liu, J. P. Zhao, Q. H. Lin and M. Lu, *Appl. Surf. Sci.*, 2019, **497**, 143760.

4 T. Y. Li, P. He, Y. N. Dong, W. C. Chen, T. Wang, J. Gong and W. L. Chen, *Eur. J. Inorg. Chem.*, 2021, **2021**, 2063-2069.

5 D. P. Dubal, B. Ballesteros, A. A. Mohite and P. Gomez-Romero, *Chemsuschem*, 2017, **10**, 731-737.

6 H. Y. Chen, R. Al-Oweini, J. Friedl, C. Y. Lee, L. Li, U. Kortz, U. Stimming and M. Srinivasan,

Nanoscale, 2015, **7**, 7934-7941.

7 G. M. Suppes, C. G. Cameron and M. S. Freund, *J. Electrochem. Soc.*, 2010, **157**, A1030-A1034.

8 Y. Y. Ge, Y. Z. Wang, G. Z. Xu, Z. G. Fang, J. F. Bai and C. Li, *J. Electroanal. Chem.*, 2023, **947**, 117779.

9 P. P. Yang, J. L. Xie, L. L. Wang, X. Y. Chen, F. K. Wu and Y. L. Huang, *Adv. Mater. Interfaces*, 2020, **7**, 2000949.

10 Y. N. Dong, L. Chen, W. L. Chen, X. T. Zheng, X. L. Wang and E. B. Wang, *Chem. - Asian J.*, 2018, **13**, 3304-3313.